Metal binding to Bacillus subtilis ferrochelatase and interaction between metal sites.

Lecerof, David; Fodje, Michel; Alvarez León, Román; Olsson, Ulf; Hansson, Andreas; Sigfridsson, Emma; Ryde, Ulf; Hansson, Mats; Al-Karadaghi, Salam

Published in:
Journal of Biological Inorganic Chemistry

DOI:
10.1007/s00775-002-0436-1

2003

Document Version:
Peer reviewed version (aka post-print)

Metal binding to *Bacillus subtilis* ferrochelatase and interaction between metal sites

David Lecerof[1], Michel N. Fodje[1], Román Alvarez León[1], Ulf Olsson[2], Andreas Hansson[2], Emma Sigfridsson[3], Ulf Ryde[3], Mats Hansson[2] and Salam Al-Karadaghi[1&]

Departments of [1]Molecular Biophysics, [2]Biochemistry and [3]Theoretical Chemistry, Center for Chemistry and Chemical Engineering, Lund University, P.O. Box 124, S-221 00 Lund, Sweden

[&])Corresponding author:

Salam Al-Karadaghi, Department of Molecular Biophysics, Center for Chemistry and Chemical Engineering, Lund University, P.O. Box 124, S-221 00 Lund, Sweden.

Tel. +46 46 2224513, fax +46 46 2224692, e-mail Salam.Al-Karadaghi@mbfys.lu.se

Abstract

Ferrochelatase, the terminal enzyme in heme biosynthesis, catalyses metal insertion into protoporphyrin IX. The location of the metal binding site with respect to the bound porphyrin substrate and the mode of metal binding are of central importance for understanding the mechanism of porphyrin metallation. In this work we demonstrate that Zn^{2+} which is commonly used as substrate in assays of the ferrochelatase reaction, and Cd^{2+}, an inhibitor of the enzyme, bind to the invariant amino acids His-183 and Glu-264 and to two water molecules, all located within the porphyrin binding cleft. On the other hand Mg^{2+}, which has been shown to bind close to the surface at 7 Å from His-183, was absent from its site. Activity measurements demonstrate that Mg^{2+} has a stimulatory effect on the enzyme, lowering K_M for Zn^{2+} from 55 to 24 μM. Changing one of the Mg^{2+} binding residues, Glu-272, to serine abolishes the effect of Mg^{2+}. It is proposed that prior to metal insertion the metal may form a sitting-atop (SAT) complex with the invariant His-Glu couple and the porphyrin. Metal binding to the Mg^{2+} site may regulate the activity by destabilising the SAT complex and stimulating porphyrin metallation.

Keywords: ferrochelatase, porphyrin metallation, metal binding, sitting-atop complex, heme synthesis

Abbreviations: SAT – sitting atop complex, *N*-MeMP -*N*-methyl mesoporphyrin

Introduction

Metals are involved in many biochemical processes, such as electron transfer, dioxygen transport and catalysis. However, they are used as true substrates in enzymatic reactions in only a few cases. One such example is the insertion of metal ions into tetrapyrroles, which results in biologically important molecules such as heme (with Fe bound), chlorophyll (Mg) and vitamin B_{12} (Co). The enzymes which catalyse the metallation reaction are commonly referred to as chelatases. Ferrochelatase, which catalyses the formation of heme by the insertion of Fe^{2+} into protoporphyrin IX (Fig. 1), is the most well-known among these enzymes [1].

X-ray crystallographic structures of ferrochelatase from three different organisms, *Bacillus subtilis* [2], human [3] and *Saccharomyces cerevisiae* [4] have been determined. The molecule has a conserved overall fold of two Rossmann-type domains with a porphyrin binding cleft between them. A similar fold has also been observed for *Salmonella typhimurium* anaerobic cobalt chelatase (Co-chelatase), demonstrating a clear evolutionary relationship between these two enzymes [5]. Both ferrochelatase and the anaerobic Co-chelatase belong to the class of ATP-independent chelatases. In contrast, the ATP-dependent chelatases, among which are the Mg-chelatase and the aerobic Co-chelatase, are composed of three different subunits and regulated by a chaperone-like AAA-type ATPase module [6, 7]. A different structural class of chelatases has recently been identified when the three-dimensional structure of Met8p, a bifunctional dehydrogenase and ferrochelatase, was determined [8].

The general mechanism of porphyrin metallation, proposed on the basis of studies of non-enzymatic systems, includes several steps: deformation of the tetrapyrrole

macrocycle, outer sphere complex formation, exchange of the coordinated solvent with the first pyrrolenine nitrogen (rate determining), chelating ring closure to form sitting-atop complex (SAT), first deprotonation of the pyrrole nitrogen by a basic solvent followed by the second deprotonation and metalloporphyrin formation [9, 10]. The three-dimensional structure of *B. subtilis* ferrochelatase in complex with a potent inhibitor and transition-state analogue *N*-methyl mesoporphyrin (*N*-MeMP) as well as with Cu-MeMP suggested a mechanism for porphyrin binding and deformation [11]. According to this mechanism the protein, by holding pyrrole rings B, C and D in a vice-like grip, forces a tilt on ring A, thereby exposing the pyrrole nitrogen to the incoming metal ion. Distortions of the porphyrin macrocycle upon binding to ferrochelatase has also been shown by Resonance Raman spectroscopy [12-14].

Although it is currently accepted that the porphyrin binds in a cleft between the two domains of ferrochelatase, the location of the metal binding site, as well as the determinants of metal specificity are still under discussion. Mutational studies on human and *S. cerevisiae* ferrochelatase suggested that an invariant histidine (His-263 and His-235, respectively) is one of the amino acid residues involved in metal binding [15, 16]. Similar indications have been obtained from X-ray absorption spectroscopy for mouse and yeast ferrochelatase (His-207 and His235, respectively) [17]. X-ray crystallography has also shown that the same histidine of the yeast and the corresponding histidine of *B. subtilis* ferrochelatase (His-183) are involved in metal binding [2, 4]. For the *S. cerevisiae* enzyme the X-ray data has also indicated that another invariant residues, Glu-314 (Glu-264 in *B. subtilis*), located in the porphyrin binding cleft, may be involved in metal binding. Its mutation in yeast and mouse ferrochelatase suggests that it is essential

for catalysis [16, 18]. A different metal binding site located close to the surface of the molecule at about 7Å from the invariant His-183 has been observed in the native as well as in the complex structure of *B. subtilis* ferrochelatase with *N*-MeMP [2, 11]. A fully hydrated Mg^{2+} ion was bound at this site. The solvent molecules were coordinated by the highly conserved amino acid residues Glu-272 and Asp-268 in a bidentate manner, by the side chain of Arg-46 and the backbone carbonyl oxygen of Glu-223 (*B. subtilis* numbering*)*. The relatively close position of this magnesium ion from His-183 suggested that the two sites may interact with each other.

In order to further investigate the mode of metal binding by ferrochelatase, understand the function of the two metal binding sites and their possible interaction, we have studied zinc and cadmium binding to *B. subtilis* ferrochelatase and the effect of magnesium on the ferrochelatase reaction assayed with zinc.

Materials and Methods

Mutagenesis, expression and purification of ferrochelatase. A mutation corresponding to a Glu-272 to serine exchange in the ferrochelatase protein was introduced by site-directed mutagenesis according to the QuikChange method (Stratagene) using *Pfu* DNA polymerase (Stratagene) and a PTC-200 DNA Engine (MJ Research). Plasmid pLUGT7-H containing the *B. subtilis hemH* ferrochelatase gene was used as template. The following primers were used; E272S_up 5´-GTGCTTTATGATAATGATTATtcATGCAAAGTGGTTACTGACG-3´, E272S_low 5´-CGTCAGTAACCACTTTGCATgaATAATCATTATCATAAAGCAC-3´. Introduced

mismatches are shown in lower case. The introduced mutation was confirmed by DNA sequencing. The recombinant wild type and E272S modified ferrochelatase were expressed and purified as described earlier [19]. During the purification process, the E272S modified ferrochelatase behaved like the wild type enzyme.

Activity measurements. Ferrochelatase activity was monitored spectrofluorometrically in a 1-ml cuvette using a Perkin Elmer Luminescence Spectrometer (LS50B). Deuteroporphyrin IX and Zn^{2+} were used as substrates. The formation of Zn-deuteroporphyrin IX was followed as an increase in emission at 577 nm using the excitation wavelength 407 nm. The excitation and emission slits were 10 nm. The 1-ml standard reaction mixture contained 100 mM Tris-HCl, pH 7.4, 0.5–5 μM deuteroporphyrin IX, 0.3 mg/ml Tween 80, 5–60 μM metal ion and 2.5 μg (71 pmol) purified ferrochelatase. The reaction was started when 500 μl of Zn-acetate was mixed with 500 μl cocktail solution containing the Tris-buffer, Tween 80, deuteroporphyrin and ferrochelatase. If Mg^{2+} was included in the measurements, $MgCl_2$ was added to the cocktail solution. A 1 mM stock solution of deuteroporphyrin IX (Sigma) was dissolved in dimethylsulfoxide. The concentration of deuteroporphyrin IX was determined from the absorbance at 398 nm in 0.1 M HCl using an absorption coefficient of 433 mM^{-1} cm^{-1}.

Crystallisation and X-ray data collection. Crystallisation of *B. subtilis* ferrochelatase was done by microseeding of sitting drops as described previously [19]. For the study of metal binding to ferrochelatase, crystals were soaked in the respective metal solution for one hour. After soaking the crystal was usually transferred to a drop containing a

cryoprotectant consisted of 18 μl reservoir solution and 2 μl PEG400. After approximately one minute the crystal was trapped with a nylon loop and flash-frozen in a stream of boiled-off nitrogen. Data were collected at station BL711 at the MAX II synchrotron, Lund, and processed with DENZO and SCALEPACK [20]. The structures were refined using CNS [21]. Data collection and refinement statistics are presented in Table 1.

Calculation of the interaction between the metal sites. To study the interaction between the two metal sites, we calculated the solvation energy of each metal in the presence or absence of the other metal using the solinprot routine of the software MEAD (Macroscopic Electrostatic with Atomic Detail) [22, 23]. This program solves the Poisson-Boltzmann equation for a protein in solvent by a finite difference method, taking into account the charges on all atoms in the protein and the detailed interface between the protein and the surrounding water. The protein was assigned a low dielectric constant of 4, whereas water had its bulk value, 80 [24]. Parse radii were used for all the atoms except for Mg^{2+} and Zn^{2+}, for which we used 2.0 Å.

The calculations were based on the 1.8 Å crystal structure of the native protein, which contains the Mg^{2+} ion [11]. The Zn-site was reconstructed into this structure by introducing a Zn^{2+} ion and its liganding solvent molecules at the position found in the metal complex. The side chains of His-183 and Glu-264 were rebuilt to the metal-bound conformation of the Zn-complex. This structure was protonated and the hydrogen atoms were equilibrated using AMBER software [25]. Standard AMBER charges were used for all atoms except for the metal sites, where the charges were

calculated with the restrained electrostatic potential model (RESP) [26] performed with AMBER software, using the standard two-stage fit. The Mg^{2+} site was modeled by six water molecules, since it is unlikely that any of the water ligands are deprotonated to a hydroxide ion, (the pK_a of Mg^{2+}-bound water is 11.4) [27]. The Zn^{2+} site was modelled by imidazole (as a model for histidine), an acetate ion (as a model for glutamate) and two water molecules. The potential points in the RESP method were sampled with the Merz-Kollman scheme in GAUSSIAN94 [28], with a high point density of about 1600 points per atom. Standard radii were used for all atoms except for Zn^{2+} and Mg^{2+}, for which a value of 2.0 Å was used [29]. The potentials were calculated with the hybrid density functional method B3LYP [30] with the 6-31G* basis set [31] for all atoms except for Zn^{2+}, for which the double-ζ basis set (62111111/33111/311) [32] was used, enhanced with diffuse p, d and f functions with exponents 0.162, 0.132 and 0.390, respectively.

Results

Metal binding to B. subtilis ferrochelatase. All ferrochelatases studied so far can, in addition to Fe^{2+}, use Zn^{2+} and often Co^{2+} as substrates *in vitro* [33]. On the other hand, many metals, among which is cadmium, inhibit the activity of the enzyme [34]. To obtain a complex, we first tried to co-crystallise ferrochelatase with Zn^{2+}. However, crystal formation was very sensitive to the presence of metal ions. Attempts to co-crystallise the protein with Zn^{2+} failed if the Zn^{2+} concentration exceeded 50 μM. However, difference electron density maps calculated using X-ray data collected from these crystals at 2.4 Å resolution did not show any high density peaks which could be unambiguously attributed to the metal. Also, longer soaking times and high metal concentrations had to be avoided,

since these led to deterioration of crystal quality. For the present work, crystals were soaked in 0.5 mM $ZnCl_2$ for one hour. Difference electron density maps undoubtedly demonstrated that Zn^{2+} was bound to the invariant residues His-183 and Glu-264. Both of these residues are located in the porphyrin binding cleft. In addition, together with the protein ligands, two solvent molecules were found to coordinate the Zn^{2+} ion, all arranged in a distorted tetrahedral geometry (Fig. 2). Metal binding distances and angles are presented in Table 2. While His-183, upon Zn^{2+} binding, essentially preserves its position of the native structure, the carboxyl group of Glu-264 is displaced by about 2 Å, leading to a disruption of hydrogen bonds to four water molecules present in the metal-free structure. One of the solvent molecules which coordinates the Zn^{2+} also makes two additional hydrogen bonds to other water molecules and to the carbonyl oxygen of the conserved residue Ser-222. The second water molecule coordinating the Zn^{2+} ion is also hydrogen bonded to Tyr-13, which has earlier been observed to be involved in an aromatic stacking interaction with the porphyrin in the ferrochelatase:*N*-MeMP structure and in interaction with Cu(II) when *N*-MeMP was metallated.

In Zn^{2+}-soaked crystals, no hydrated Mg^{2+} ion could be detected at the site where it was observed earlier (the outer site). The conformation of the amino acid side chains, involved in coordinating the solvent molecules that interact with the Mg^{2+} ion, were essentially identical in the two structures. The superposition of the Zn^{2+}-soaked and native structures gave an rms deviation of the Cα atoms of 0.18 Å. Only one noticeable difference between the two structures was observed, in the flexible region Pro-16-Pro-55, which has moved by around 0.3 Å in a direction that slightly widened the porphyrin

binding cleft. In contrast, porphyrin binding led to larger rearrangements of the protein conformation in this region with shifts in C_α atoms of up to 8 Å [11].

The refinement of the occupancy of the Zn^{2+} resulted in a value of 0.94. In our attempts to achieve higher resolution of the X-ray data, we collected two other data sets with other Zn^{2+} concentrations and soaking times. The structure and metal occupancy were subsequently refined against each of these data sets. For 30 minutes of soaking in 0.25 mM Zn^{2+} solution (resolution 2.1 Å) a value for the occupancy of 0.45 was obtained, while 20 min soaking in 0.5 mM metal solution (resolution 2.4 Å) resulted in an occupancy of 0.75. Thus, despite the relatively high metal concentrations in the soaking solution, the occupancy of the site was relatively low.

In order to compare the binding of a substrate metal, Zn^{2+}, with binding of an inhibitor, we collected new synchrotron data to high resolution (2.2 Å) from crystals soaked with Cd^{2+}. We found two sites to which the metal binds with considerable occupancy. One site was similar to that found for Zn^{2+}, where the cadmium ion was coordinated by His-183, Glu-264 and two solvent molecules, although the distances to Glu-264 and the solvent were longer than for Zn^{2+}, (Table 2). The second site was located at approximately 9Å from the first. In this case the metal is coordinated by His-262 and 3 solvent molecules.

The effect of Mg^{2+} on B. subtilis ferrochelatase activity. During the crystallisation of *B. subtilis* ferrochelatase Mg^{2+} was present in the buffer solution. The initial concentration of Mg^{2+} in the drops was usually 0.1 M, but crystals could form within the range of 0.05–0.5 M Mg^{2+}. The need for Mg^{2+} for crystallisation is not understood, but its binding in

close vicinity to the other metal binding site and the porphyrin led us to test its effect on the catalytic reaction. Zn^{2+} and deuteroporphyrin IX were used as substrates in the ferrochelatase assay and the formation of Zn-deuteroporphyrin IX was monitored as an increase in fluorescence emission at 577 nm. Four mM Mg^{2+} was used in the analysis, which is in the range of the physiological concentration in many cells [35]. Mg^{2+} had a stimulatory effect on the activity and lowered the K_M of Zn^{2+} from 55 to 24 μM (Fig. 3A). The K_M of deuteroporphyrin appeared unaffected. The same analysis was performed with ferrochelatase which had an E272S modification. As mentioned above, Glu-272 is involved in the coordination of the Mg^{2+} ion via a solvent molecule. Compared to the wild type enzyme, this mutation reduced V_{max} by half, slightly increased K_M for deuteroporphyrin, but had no effect on K_M for Zn^{2+}. The addition of 4 mM Mg^{2+} to the assay did not effect the kinetic parameters of the E272S modified enzyme (Fig. 3B). This shows that the stimulatory effect of Mg^{2+} depends on the presence of an intact magnesium-binding site, and that the two metals at the two sites can interact with each other. Screening of other ions showed that Ca^{2+} had an effect similar in magnitude to that of Mg^{2+} (not shown).

A model for the interaction between the two metal binding sites. Model calculations also show that Mg^{2+} and Zn^{2+} at the observed locations interact with each other, mutually reducing the metal binding affinity of the sites. Electrostatic interactions between the sites in the presence of Zn^{2+} and Mg^{2+} were studied by calculating the relative binding energies to the protein for the Zn^{2+} ion in the presence and absence of Mg^{2+}, and *vice versa*. In the calculations with the Mg^{2+} ion, quantum chemical charges were used for

Mg^{2+} and its water ligands. When Mg^{2+} was not present, the charge of the Mg^{2+} ion was set to zero and the charges of the water ligands were set to standard Amber charges. The Zn^{2+} site was treated analogously.

The calculations predicted the Zn^{2+} ion to bind with 15 kJ/mol lower affinity in the presence of Mg^{2+}, while the Mg^{2+} ion would bind with 25 kJ/mol lower affinity when Zn^{2+} was bound. This is an effect of the electrostatic repulsion of two ions with similar charges, screened by the surrounding protein side chains and solvent (in a vacuum, the repulsive interaction would be almost 800 kJ/mol at this distance; fully screened in water solution it would be 9 kJ/mol). The results indicate that the presence of one ion in the protein would decrease the binding constant of the other ion by a factor of about 1000, which may explain the mutual effects of Mg^{2+} and Zn^{2+} observed in our experiments.

Discussion

The data presented here show that the mode of metal binding in ferrochelatase is more complex than has been believed, and may involve two interacting metal binding sites. Thus, soaking of *B. subtilis* ferrochelatase with Zn^{2+} and Cd^{2+} revealed a metal bound to a site located in the porphyrin binding cleft (the inner site). This site, as shown by the structure of the complex of *B. subtilis* ferrochelatase with *N*-MeMP [11], is in close vicinity to the distorted pyrrole ring A, which had its nitrogen directed towards His-183 and Glu-264, the main metal coordinating amino acids. Also in *S. cerevisiae* ferrochelatase the substrate metal, Co^{2+}, as well as Cd^{2+} were bound to a residue corresponding to His-183, namely His-235 at approximately 2.0 Å and to Glu-

314 (corresponds to Glu-264) at 2.8 Å. The identification of the invariant His-Glu couple as the main amino acid residues responsible for metal binding agrees with the previous studies which demonstrated that these residues are essential for metal binding and activity [15-18].

The short distance from the metal to the histidine indicates that this residue is the primary contributor to metal binding in both yeast and *B. subtilis* ferrochelatase. The distances to the glutamate and solvent are longer, with only one solvent molecule in the Zn-complex being an exception (positioned at 2 Å from the zinc). A superposition of the Zn^{2+} ion on the structure of the complex of ferrochelatase with *N*-MeMP (Fig. 4A) shows that this mode of metal binding would allow the porphyrin to bind without interfering with the metal coordinating residues, His-183 and Glu-264. Judged from the structures, the metal will be at 2.6 Å from the pyrrole nitrogen, a distance sufficient for the formation of the first metal-nitrogen bond. The solvent, which coordinate the zinc, will presumably be displaced by the porphyrin. Analysis of the structure also suggests that the metal, if bound to the outer site, may easily be channelled to the active site (the inner site) by a group of conserved acidic residues (Fig. 4A). A similar arrangement can be found in the structure of the distantly related Co-chelatase (Fig. 4B). Interestingly, the acidic residues are aligned along a rare secondary structure element, a π-helix [36], conserved in all ferrochelatases and in Co-chelatase (Fig. 4C). Such residue alignment would only be possible for a π- and a 3_{10}-helix. However, in the case of a 3_{10}-helix the unit rise per residue (2.0 Å) is twice as large as for a π-helix, which will result in a longer distance between side chains. This model may also provide an explanation for the stimulation of ferrochelatase activity by Mg^{2+}. Thus, the repulsion between the metals at

the inner and the Mg-binding sites (the outer site), by lowering the affinity of the inner site for metal, would facilitate metal insertion into the porphyrin.

The additional Cd^{2+}-binding site found in this work may account for the inhibitory effect of the metal by interfering with porphyrin and/or metal binding at the active site. Also in the yeast enzyme cadmium was bound at a second sites, although it was located close to the surface at approximately 12 Å from the conserved Glu-His couple. No indication could be found of a metal bound to a site described for the human ferrochelatase [3, 37]. In this study the metal (Co^{2+}) was bound at approximately 20 Å from the invariant His-Glu couple. The residues coordinating the metal, His-230 and Asp-383, correspond to *B. subtilis* residues Glu-150 and Thr-302. It should also be mentioned that in the human ferrochelatase structure 3 detergent molecules were bound in the porphyrin binding cleft in immediate vicinity of the His-Glu. This will most probably prevent the metal from binding within the porphyrin binding cleft.

Thus, the special structural features of the region around the Mg-binding site may play an important role in the function of ferrochelatase, and presumably in the function of other chelatases of this class.

Acknowledgements. The authors are grateful to Anders Liljas for helpful discussions. This work was supported by grants from the Swedish Natural Science Research Council to SA and the Swedish Council for Forestry and Agricultural Research and *Carl Tryggers Stiftelse för Vetenskaplig Forskning* to MH.

Figure legends

Fig. 1 Ferrochelatase catalyses the formation of heme (protoheme IX) by insertion of a ferrous ion into protoporphyrin IX.

Fig. 2 Zinc binding to ferrochelatase. Metal coordination distances and angles are shown in Table 2

Fig. 3 Lineweaver-Burk plots of Zn^{2+}-chelatase activity measured with ferrochelatase, and the effect of 4 mM Mg^{2+} on this activity (open symbols, with Mg^{2+}; filled symbols, without Mg^{2+}). Ferrochelatase wild type enzyme (**A**) and an E272S mutant ferrochelatase (**B**) were used. The lines represent measurements with different concentrations of deuteroporphyrin IX (squares, 0.5 μM deuteroporphyrin; circles, 0.65 μM; standing triangles, 0.91 μM; hanging triangles 1.54 μM; stars, 5.0 μM). The K_M and V_{max} values were calculated from secondary plots. Wild type ferrochelatase without Mg^{2+}: V_{max} 1.0 μmol min^{-1} mg^{-1}, K_M Zn^{2+} 55 μM, K_M deuteroporphyrin IX 1.0 μM. Wild type ferrochelatase with Mg^{2+}: V_{max} 1.4 μmol min^{-1} mg^{-1}, K_M Zn^{2+} 24 μM, K_M deuteroporphyrin IX 1.2 μM. E272S ferrochelatase without Mg^{2+}: V_{max} 0.56 μmol min^{-1} mg^{-1}, K_M Zn^{2+} 54 μM, K_M deuteroporphyrin IX 1.4 μM. E272S ferrochelatase with Mg^{2+}: V_{max} 0.55 μmol min^{-1} mg^{-1}, K_M Zn^{2+} 50 μM, K_M deuteroporphyrin IX 1.6 μM.

Fig. 4 A common feature of ferrochelatase and Co-chelatase is a π-helix n with acidic amino acids which form a path from the surface of the protein to the active site. In

B. subtilis ferrochelatase (**A**), and also in *S. typhimurium* Co-chelatase (**B**), this region is binds ion complexes. In ferrochelatase a fully hydrated Mg^{2+} ion, seen in (**A**), is located at approximately 7 Å from the invariant His-183. In Co-chelatase, the authors have built a sulfate ion into this site. The Zn^{2+} ion (shown in magenta), as found in the Zn^{2+}-ferrochelatase complex, and the side chain of Glu-264 (cyan), coordinating the zinc, are also shown in (**A**). (**C**) A superposition of the π-helices from *B. subtilis*, human and yeast ferrochelatse as well as Co-chelatase.

Table 1. Data collection and refinement statistics for Zn^{2+} and Cd^{2+} soaked into native ferrochelatase.

	Zn^{2+}	Cd^{2+}
Data collection:		
[1]Cell, a, b, c (Å)	48.68, 49.88, 118.53	48.42,49.88,118.78
Resolution range (Å)	15-2.6	15-2.2
[2]Completeness (%)	95.9 (97.4)	97.3 (96.7)
Unique reflections	9203	15512
$I/\sigma(I) > 3$ (%)	79.1 (57.2)	91.2 (80.0)
[3]R_{merge} (%)	12.8 (34.2)	24.1
Refinement:		
No. protein atoms	2486	2486
No. water molecules	41	122
[4]R_{cryst} (R_{free})	21.7 (27.4)	24.6 (29.6)
Rmsd from ideality		
bond length (Å)	0.008	0.007
bond angles (°)	1.35	1.22
dihedrals (°)	21.3	21.1
Average B-factors ($Å^2$)		
side chain	27.9	15.8
main chain	23.8	13.6

[1]Space group $P2_12_12_1$

[2]The numbers in parentheses are for the highest resolution shell.

[3]$R_{merge} = \Sigma_i|I-\langle I\rangle|/\Sigma_i(I)$.

[4]$R_{cryst} = \Sigma|F_{obs} - F_{calc}| / \Sigma F_{obs}$, where F_{obs} and F_{calc} are the observed and calculated structure factor amplitudes, respectively. R_{free} is calculated on 10% of the data, which were excluded from refinement.

Table 2. Distances and angles between the metals (Zn^{2+} and Cd^{2+}) and their ligands.

	Zn^{2+}	Cd^{2+}
Distance (Å)		
His-183 Nε2	2.1	2.2
Glu-264 Oε1	2.2	2.7
[1]Wat	2.3	2.9
[2]Wat	2.0	3.1
Angles (°)		
His-183 (Nε2)-Me-(Oε1) Glu-264	90	103
His-183 (Nε2)-Me–Wat	86	158
His-183 (Nε2)-Me-Wat	95	103
Glu-264 (Oε1)-Me-Wat	106	146
Glu-264 (Oε1)-Me-Wat	120	85
Wat-433-Me-Wat	134	79

[1]This water is H-bonding to the hydroxyl group of Tyr-13.

[2]This water is H-bonding to the carbonyl oxygen of Ser-222.

Reference List

[1] Dailey HA, Dailey TA, Wu CK, Medlock AE, Wang KF, Rose JP, Wang BC (2000) Cell Mol Life Sci 57: 1909-26.

[2] Al-Karadaghi S, Hansson M, Nikonov S, Jönsson B, Hederstedt L (1997) Structure 5: 1501-1510.

[3] Wu CK, Dailey HA, Rose JP, Burden A, Sellers VM, Wang BC (2001) Nat Struct Biol 8: 156-160.

[4] Karlberg, T., Lecerof D, Gora M, Silvegren G, Labbe-Bois R, Hansson M, Al-Karadaghi S (2002) Biochemistry In press.

[5] Schubert HL, Raux E, Wilson KS, Warren MJ (1999) Biochemistry 38: 10660-10669.

[6] Raux E, Schubert HL, Warren MJ (2000) Cell Mol Life Sci 57: 1880-1893.

[7] Fodje MN, Hansson A, Hansson M, Olsen JG, Gough S, Willows RD and Al-Karadaghi S (2001) J Mol Biol 311: 111-122.

[8] Schubert HL, Raux E, Brindley AA, Leech HK, Wilson KS, Hill CP, Warren MJ (2002) EMBO J 21: 2068-2075.

[9] Lavallee DK (1985) Coord Chem Rev 61: 55-96.

[10] Inamo M, Kamiya N, Inada Y, Nomura M, Funahashi S (2001) Inorg Chem 40: 5636-5644.

[11] Lecerof D, Fodje M, Hansson A, Hansson M, Al-Karadaghi S (2000) J Mol Biol 297: 221-232.

[12] Blackwood MEJ, Rush TS3, Romesberg F, Schultz PG, Spiro TG (1998) Biochemistry 37: 779-782.

[13] Franco R, Ma JG, Lu Y, Ferreira GC, Shelnutt JA (2000) Biochemistry 39: 2517-2529.

[14] Lu Y, Sousa A, Franco R, Mangravita A, Ferreira GC, Moura I, Shelnutt JA (2002) Biochemistry 41: 8253-8262.

[15] Kohno H, Okuda M, Furukawa T, Tokunaga R, Taketani S (1994) Biochim Biophys Acta 1209: 95-100.

[16] Gora M, Grzybowska E, Rytka J, Labbe-Bois R (1996) J Biol Chem 271: 11810-11816.

[17] Ferreira GC, Franco R, Mangravita A, George GN (2002) Biochemistry 41: 4809-4818.

[18] Franco R, Pereira AS, Tavares P, Mangravita A, Barber MJ, Moura I, Ferreira GC (2001) Biochem J 356: 217-222.

[19] Hansson M, Al-Karadaghi S (1995) Proteins 23: 607-609.

[20] Otwinowski Z, Minor W (1997) Meth Enzymology 276: 307-326.

[21] Brunger AT, Adams PD, Clore GM, DeLano WL, Gros P, Grosse-Kunstleve RW, Jiang JS, Kuszewski J, Nilges M, Pannu NS, Read RJ, Rice LM, Simonson T, Warren GL (1998) Acta Crystallogr D Biol Crystallogr 54: 905-921.

[22] Bashford D, Gerwert K (1992) J Mol Biol 224: 473-486.

[23] Ishikawa Y, Oldehoeft RR, Reynders JVW and Tholburn M (1997) Lecture Notes in Computer Science. Springer, Berlin.

[24] Honig B, Nicholls A (1995) Science 268: 1144-1149.

[25] Pearlman DA, Case DA, Caldwell JW, Ross WS, Ferguson DM, Seibel GL, Singh UC, Weiner PK, Kollman PA (1995) AMBER 4.1. University of California, San Francisco.

[26] Bayly CI, Cieplak P, Cornell WD, Kollman PA (1993) J Phys Chem 97: 10269-10280.

[27] Zheng YJ, Bruice TC (1997) J Am Chem Soc 119: 8137-8145.

[28] Frisch, M. J., Trucks, G. W., Schlegel, H. B., Gill, P. M. W., Johnson, B. G., Robb, M. A., Cheeseman, J. R., Keith, G. A., Petersson, T., Montgomery, J. A., Raghavachari, K., Al-Laham, M. A., Zakrzewski, V. G., Ortiz, J. V., Foresman, J. B., Cioslowski, J., Stefanov, B. B., Nanayakkara, A., Challacombe, M., Peng, C. Y., Ayala, P. Y., Chen, W., Wong, M. W., Andres, J. L., Replogle, E. S., Gomperts, R., Martin, R. L., Fox, D. J., Binkley, J. S., Defrees, D. J., Baker, J., Stewart, J. P., Head-Gordon, M., Gonzalez, C., Pople, JA (1995) Gaussian. Gaussian Inc, Pittsburgh PA.

[29] Sigfridsson E, Ryde U (1998) J Comput Chem 19: 377-395.

[30] Barone V (1994) Chem Phys Lett 226: 392-398.

[31] Hehre WJ, Radom L and Scheyer P.V.R.and Pople JA (1986) Ab Initio Molecular Orbital Theory. Wiley-Interscience, New York.

[32] Schafer A, Horn H and Ahlrichs R (1992) J Chem Phys 97: 2571-2577.

[33] Jordan PM and Dailey H (1990) Mol Aspects Med 11: 21-23.

[34] Dailey HA (19870) Ann NY Acad Sci 514: 81-86.

[35] Cowan JA (1991) The Biological Chemistry of Magnesium. VCH Publishers, Inc., New York.

[36] Fodje M, Al Karadaghi S (2002) Protein Eng 15: 353-358.

[37] Sellers VM, Wu CK, Dailey TA, Dailey HA (2001) Human ferrochelatase: characterization of substrate-iron binding and proton-abstracting residues. Biochemistry 40: 9821-9827.

Fig. 1
Lecerof et al.

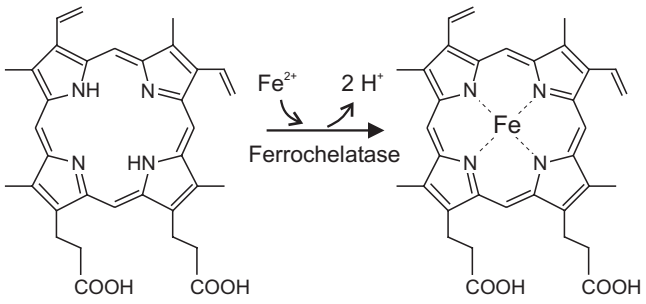

Protoporphyrin IX

Protoheme IX
(Heme b)

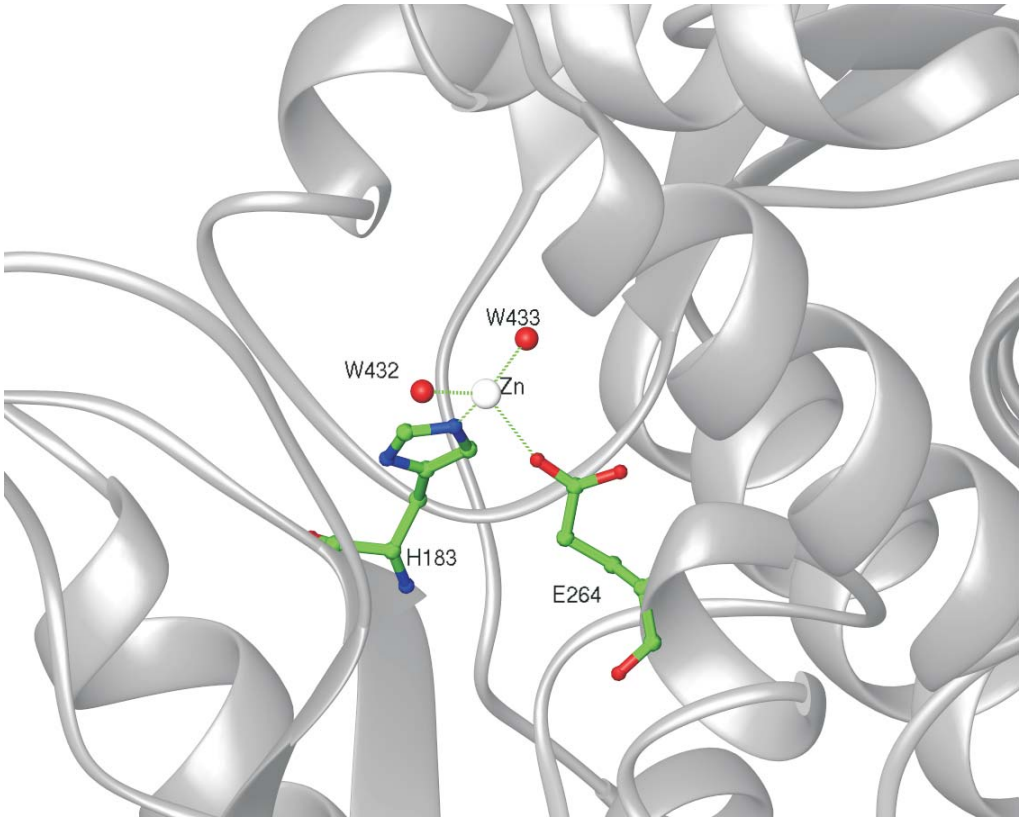
W433
W432
Zn
H183
E264

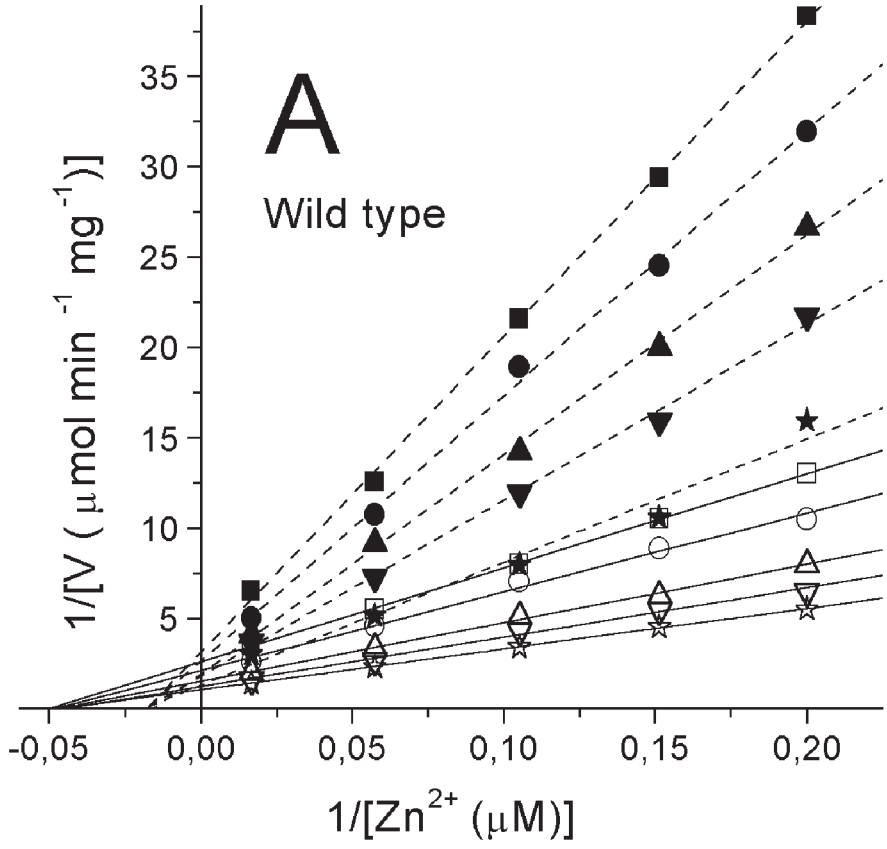
A
Wild type
1/[V (μmol min -1 mg -1)]
35
30
25
20
15
10
5
-0,05
0,00
0,05
0,10
0,15
0,20
1/[Zn2+ (μM)]

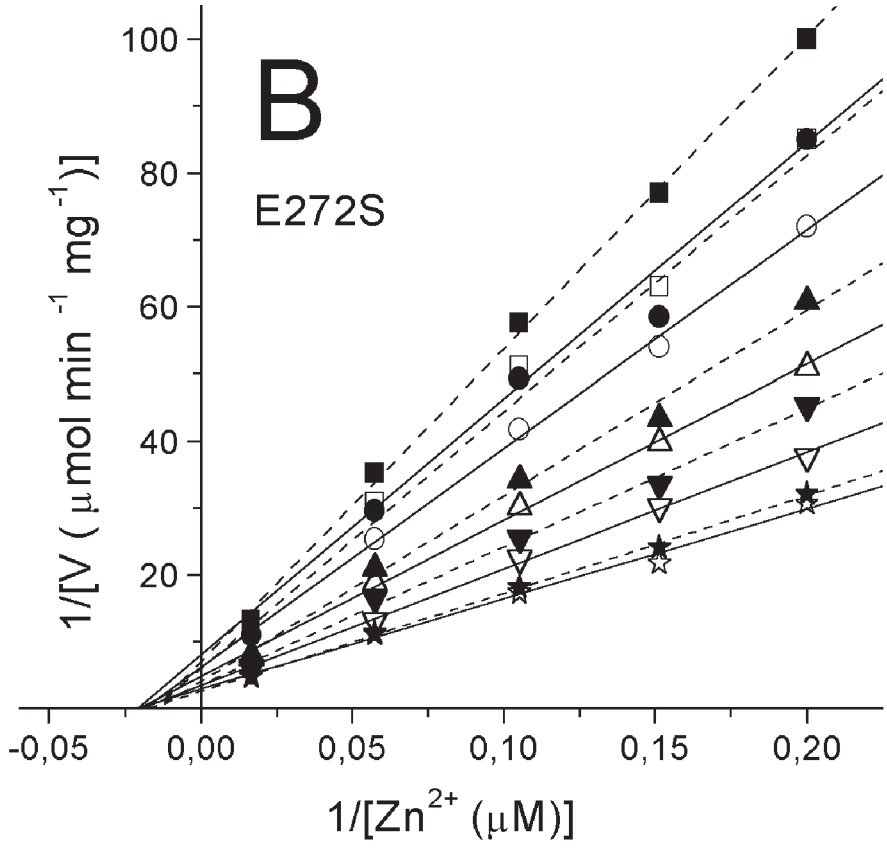
B
E272S
1/[V (μmol min -1 mg -1)]
100
80
60
40
20
-0,05
0,00
0,05
0,10
0,15
0,20
1/[Zn2+ (μM)]

A

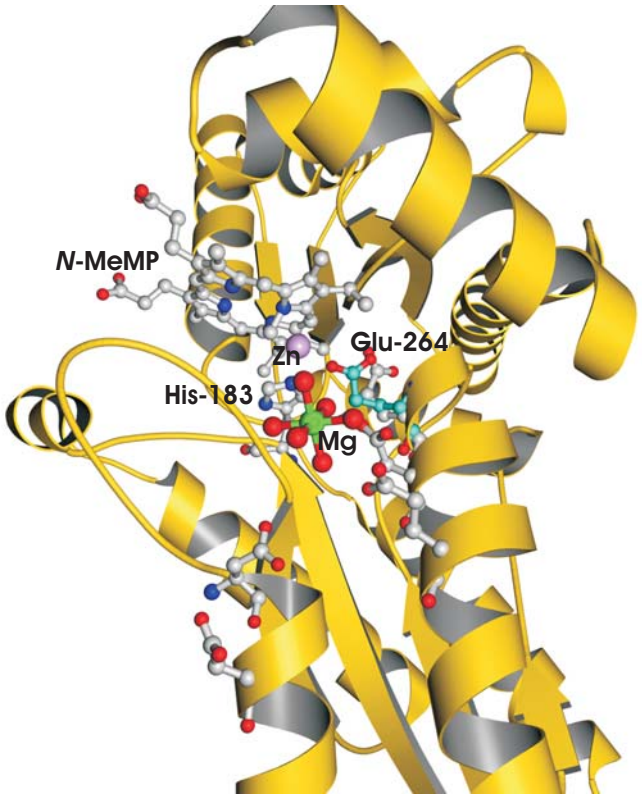

C

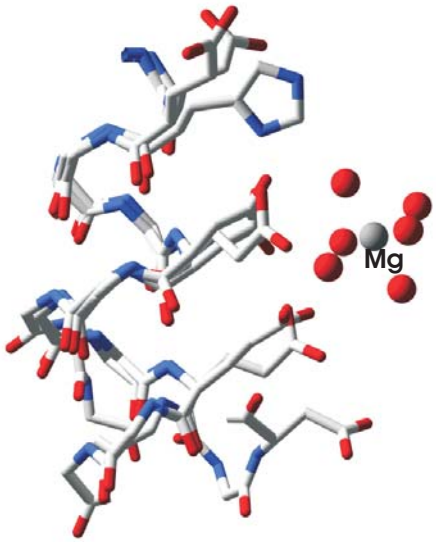

B

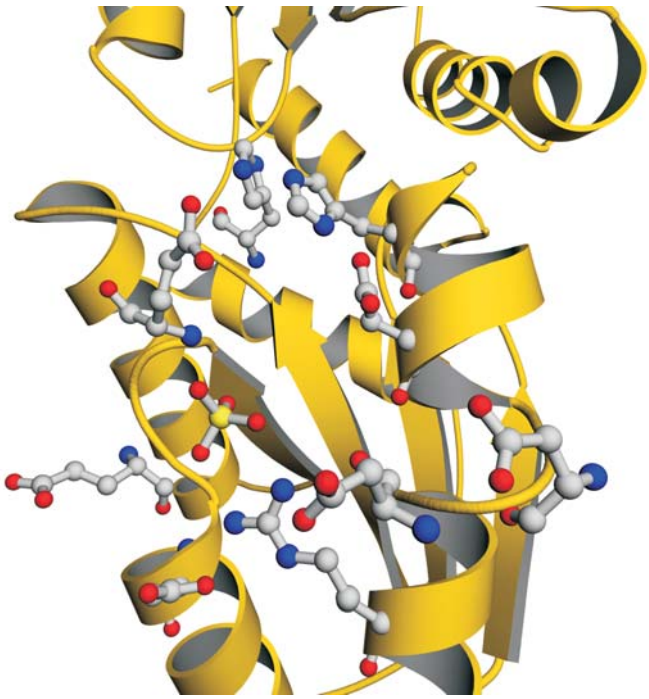

Lecerof et al., Fig. 4